Radio Science, Volume 15, Number 6, pages 1149–1161, November–December 1980

Transmission line model of the interaction of a long metal wire with the ionosphere

D. A. Arnold and M. Dobrowolny[1]

Smithsonian Astrophysical Observatory, Cambridge, Massachusetts

(Received July 12, 1979; revised March 21, 1980; accepted April 10, 1980.)

An equivalent electric circuit model is used to study the electrodynamic interactions of long orbiting metallic tethers with the ionospheric plasma and, in particular, to derive current and potential profiles along bare metallic tethers. In contrast with other models, this approach is dynamic, enabling both the transient behavior of the wire and its final equilibrium state to be derived. A comparison with the results of other models indicates the advantage of the present approach, especially in those cases where the internal resistance of the tether plays a major role in determining the current and potential distributions.

1. INTRODUCTION

The electrodynamic interactions of long metallic tethers in the ionospheric plasma have been the subject of some recent studies [*Dobrowolny,* 1978; *Morrison et al.,* 1979]. Such studies consider the equilibrium state of the tether and derive current and voltage profiles for bare metallic tethers, taking into account the effect of the wire resistance R. In the case of *Dobrowolny* [1978], a numerical procedure is developed, starting with the current and voltage profiles for a perfectly conducting tether ($R = 0$), which are derived by imposing no net accumulation of charge on the tether. Then a small resistance is introduced in the ordinary Ohm's law and gradually increased until the profiles in presence of the actual tether resistance are obtained. On the other hand, *Morrison et al.* [1979] use a simplified model for particle collection and derive a differential equation for the potential, which is amenable to an analytical solution.

The present work differs from the previous ones in that it is a dynamic formulation that derives the equilibrium state of the wire as the end product of the dynamic evolution of the system, starting from a set of initial conditions. More specifically, the model is based on an electric circuit equivalent of the tether, in which the electric charge at a set of points along the tether is obtained as a function of time by numerical integration of the equations giving the rate of change of charge at each point. This approach allows the transient behavior of the wire to be obtained, as well as the equilibrium state.

This new method of computing charge distribution on a tether has been added to a large computer model that calculates the dynamics of long wires in space, taking into account the effects of electrodynamic forces (induction drag) on the various elements of the wire [*Anderson et al.,* 1979].

Rather than going into details of the dynamical motions of the wire, we limit ourselves to the derivation of current and potential profiles for a moving tether assumed to be in a straight line configuration. Also, as in the previously quoted works, we implicitly assume a negligible impedance of the circuit external to the tether. The consideration of such circuit is at this moment a quite open problem [see *Drell et al.,* 1965; *Dobrowolny et al.,* 1979].

The plan of the presentation is the following: an explanation of the equivalent circuit of the tether and of the computational method used is given in section 2. Section 3 gives some results on the transient buildup of potential and currents in a metallic tether coated with dielectric. This dynamical case could not be reproduced by any of the previous methods. Section 4 obtains current and potential profiles in equilibrium for a bare metallic tether and discusses them as a function of the tether's internal resistance. The comparison of these results with those of previous methods (section 5) leads to criticisms of such methods and indicates the advantage of the present formulation, especially in situations where the tether's internal resistance

[1]Permanent address: Laboratorio Plasma Spazio, CNR Frascati 00044, Italy.

Paper number 80S0493.
0048-6604/80/1112-0493$01.00

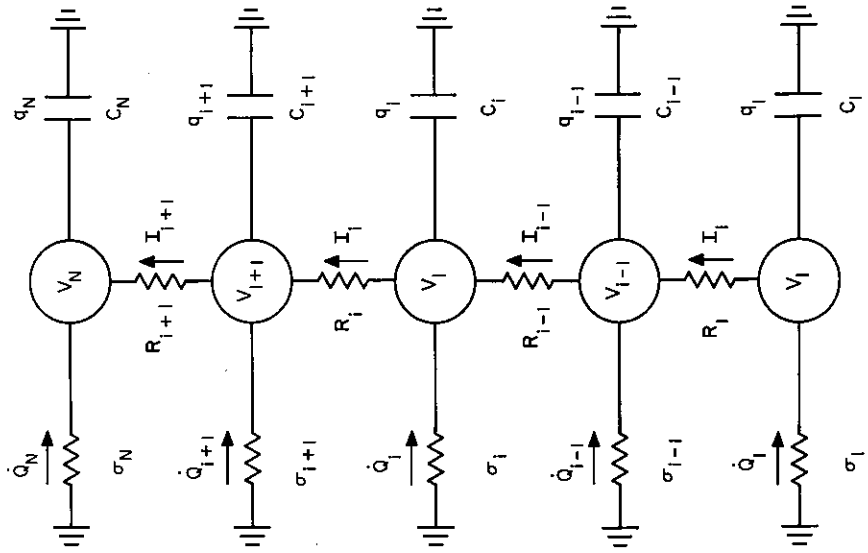

Fig. 1. Equivalent electric circuit of an orbiting wire.

is high and therefore crucial in determining the current and potential profiles.

2. EQUIVALENT ELECTRIC CIRCUIT OF THE ORBITING WIRE

The tether has been modeled as a conducting cylinder with distributed resistance and capacitance. Although inductance could also be included, it has not been because of the low value of the inductive reactance per unit length compared to the other reactances. The electrical state of the wire is specified by giving the electric charge on each of the discrete points representing the wire. The electric charge as a function of time is obtained by numerical integration of an equation giving the rate of change of charge at a given point. If inductance were included, it would also be necessary to integrate the current by using an expression for its rate of change.

The transmission line model of the orbiting wire uses the equivalent electric circuit, shown in Figure 1, to represent the wire itself. Each node in the circuit diagram represents the lumped properties of a section of the wire. Thus we associate with node i a resistor R_i and a capacitor C_i, as indicated. Besides, one must include a conductance σ_i, which represents the leakage current $\dot{Q}_i$ from the plasma to node i. This is a nonlinear function of the electrostatic potential V_i due to the charge q_i:

$$\dot{Q}_i = f(V_i) \tag{1}$$

which we will discuss and give explicitly in sections 3 and 4. In turn, the potential V_i is obtained from

$$V_i = q_i / C_i \tag{2}$$

The calculation of the circuit analogue of Figure 1 proceeds in the following way. Charges q_i are initially given (at $t = 0$) on the capacitors C_i. The further time evolution of such charges is then computed by integrating the equation

$$dq_i/dt = I_{i-1} - I_i + \dot{Q}_i \tag{3}$$

where the internodal current I_i is obtained from Ohm's law:

$$I_i = [(V_i - V_{i+1}) + (\mathbf{v}_i \times \mathbf{B}_i + \mathbf{E}_i) \cdot \Delta\mathbf{l}_i]/R_i \tag{4}$$

Here $\mathbf{v}_i = \mathbf{V}_{\text{orb},i} - \mathbf{V}_{\text{rot}}$, where $\mathbf{V}_{\text{orb},i}$ is the orbital velocity of the node (i.e., the shuttle velocity of $\sim$7.7 km/s) and $\mathbf{V}_{\text{rot}}$ is the rotational velocity of the magnetic field (equal to the earth's rotational speed of $\sim$0.46 km/s). Furthermore, $\mathbf{E}_i$ represents an ionospheric electric field perpendicular to the lines of force of the earth's magnetic field, and $\Delta\mathbf{l}_i$ is the distance between the $i + 1 -$ th and the ith node. After a transient phase the solutions of (3) converge to an equilibrium where $\dot{q}_i = 0$, and hence the sum of the currents into each node is zero (this, in fact, provides a check on having converged to equilibrium in the computation). The

duration and features of the transient dynamical phase depend, of course, on the values which are given to the capacitors C_i. On the other hand, the equilibrium distribution of charges and currents are, of course, independent of such capacitance values. The capacitance C_i would be easily calculated for the particular case of a metallic tether coated with dielectric. There we could write

$$C_i = C\Delta l_i \tag{5}$$

and use for the capacitance per unit length C, the following expression:

$$C = [2\pi\varepsilon_0/ln(r_2/r_1)] \tag{6}$$

where r_1 is the radius of the metallic tether (without coating) and r_2 the radius of the coated tether (external radius). Capacitance is, on the other hand, not so easily calculated for the case of a bare metallic tether because of the difficulty of calculating the radial distribution of electric field surrounding the tether. In the following we will give for the case of a bare metallic tether only equilibrium results and use in these calculations (5) and (6), with $r_2 - r_1$ of the order of the Debye length (although the dimension of the sheath surrounding the tether can be much larger than this for the case of high potential, this choice will not affect the equilibrium quantities).

A different approach of computation is followed to deal with the idealized case of a perfectly conducting tether ($R = 0$), by which we mean, more physically, a value of resistance so small that it is not affecting the equilibrium values of potential and current along the tether.

For the case $R = 0$, (3) cannot be used, and in fact, the approach previously described in the limit $R \to 0$ would be giving a transient phase of infinitesimal duration $\Delta t \to 0$, where the current value goes to infinity. Physically, what happens when a wire of negligible resistance is placed into orbit is that the electrons in the wire immediately ($\Delta t \to 0$) redistribute themselves until the forces that are due to charge buildup balance the external forces arising from the electric and magnetic fields. The equilibrium state is not, however, characterized by an infinite current value and, in fact, is determined not by Ohm's law but by the condition of no net charge accumulation on the tether. This means that

$$\Sigma\dot{Q}_i = 0 \tag{7}$$

As, in such a perfectly conducting case, there is only leakage to the plasma, one has $\Sigma\dot{Q}_i = \Sigma\dot{q}_i$, and hence differentiating (2),

$$\Sigma\dot{Q}_i = \Sigma C_i\dot{V}_i \tag{8}$$

On the other hand, from (4), in the limit $R_i \to 0$ and in order to have a finite current, we obtain the relation

$$V_i - V_{i+1} + (\mathbf{v}_i \times \mathbf{B}_i + \mathbf{E}_i) \cdot \Delta\mathbf{l}_i = 0 \tag{9}$$

which in the case of a straight wire configuration just says that the potential, in the absence of ohmic losses, is linearly distributed along the wire. As potential differences are fixed by (9), $\dot{V}_i$ will be the same for all nodes, and therefore from (8),

$$\dot{V}_i = \Sigma\dot{Q}_i/\Sigma C_i \tag{10}$$

The equilibrium configuration for a perfectly conducting wire is thus determined by starting from an initial value of the potential at one node. Then (9) gives the initial potential at all other nodes, and (10), with such values as initial conditions, follows the potential V_i as a function of time until all $\dot{V}_i$'s go to zero. The search for this final state (as is seen more clearly for the case of a straight wire) is equivalent to a search for the point of the tether at zero potential with respect to the plasma.

For any equilibrium potential distribution the current I_i in the wire is obtained as follows: for the first node, $\dot{I}_1 = \dot{Q}_1 - \dot{q}_1$, where $\dot{q}_1 = C_1\dot{V}_1$. The current in the rest of the wire can be obtained by using the following equation:

$$I_i = I_{i-1} + \dot{Q}_i - \dot{q}_i$$

at successive nodes.

The above formulation for the problem of current and potential distribution in a perfectly conducting tether is quite general and can be used for any position assumed by the tether in the course of its orbiting in the ionosphere, i.e., for any velocity and orientation with respect to the magnetic field of the various lumped segments of the tether.

In the cases to be presented here, we will, however, refer to the simpler situation of a straight wire aligned with the z axis, with the lower end at the origin, moving at constant velocity $\mathbf{v}_0$ perpendicular to a constant magnetic field $\mathbf{B}$ (see Figure 2). We also assume that the natural electrostatic field in the ionosphere is negligible. For such geometry, and referring again to the $R = 0$ case, any

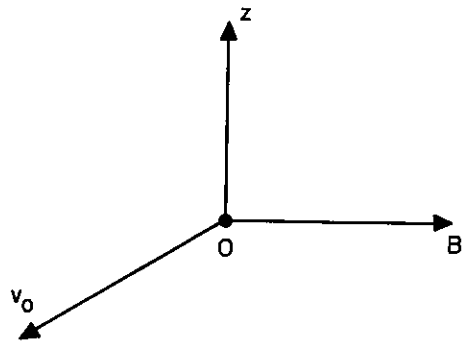

Fig. 2. Geometry of the tether's motion with respect to the earth's magnetic field.

charge collected along the perfectly conducting wire is immediately distributed so as to maintain a linear voltage distribution. In such a case, (9) becomes

$$V_i = Bv_0(z_i - z_0) = q_i/C_i \tag{11}$$

where z_0 is the point where the wire is at plasma potential. For eastward motion of the tether the upper end will be positive with respect to the lower end.

The rate of change of z_0 depends on the rate of change of the total charge of the wire and can thus be obtained from (11) as

$$\dot{z}_0 = -\sum_i \dot{q}_i \Big/ Bv_0 \sum_i C_i \tag{12}$$

This equation for $\dot{z}_0$ can be used to determine z_0 as a function of time, starting from some initial value.

3. TRANSIENT BUILDUP OF CHARGES AND CURRENTS IN A METALLIC TETHER COATED WITH DIELECTRIC

We consider here a metallic tether coated with dielectric. Charges are collected from the plasma at two conducting electrodes at the end, which in the calculations we took as spheres. In practice, in space applications these could be the conducting part of the Shuttle at one end and a conducting balloon on the other. In the steady state, one has a constant current and a linear potential distribution

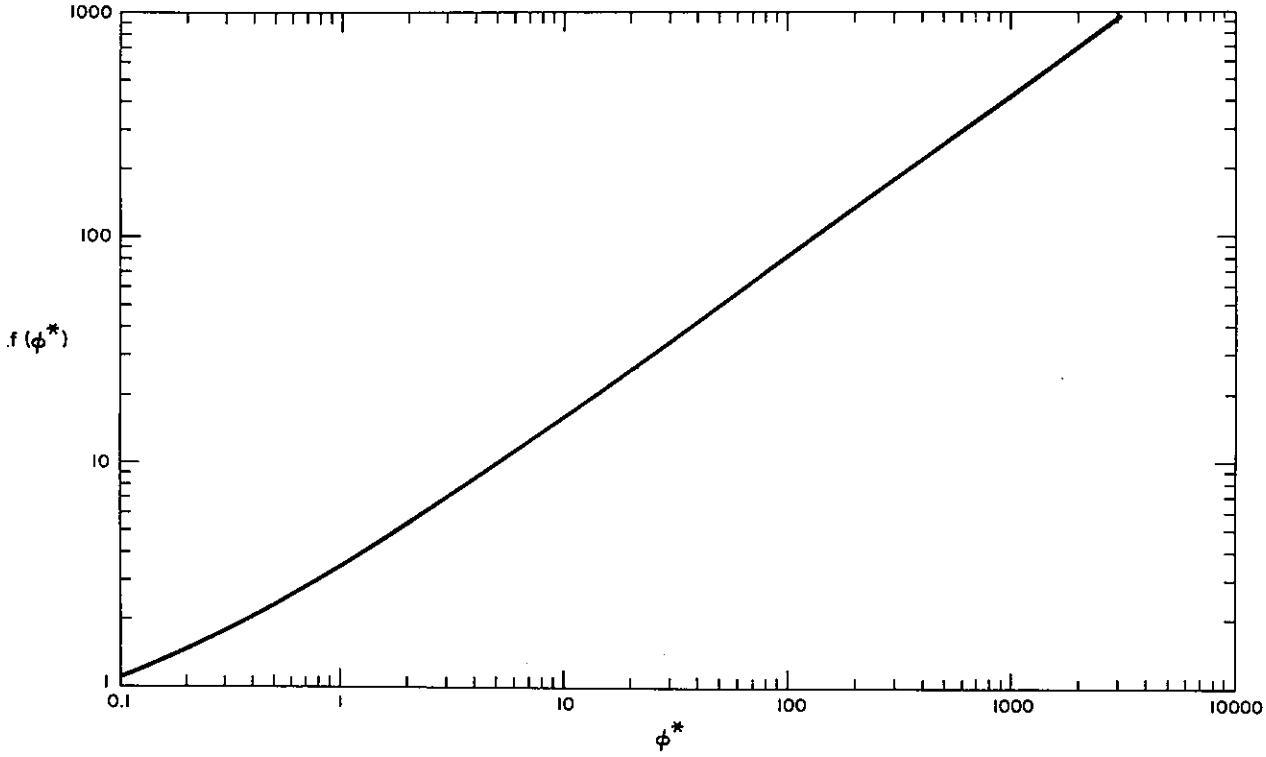

Fig. 3. Plot of the function $f(\phi^*)$ (see (13)) defining the collection efficiency of spherical electrodes.

along the tether. We will show some examples of the transient approach to such a steady state, obtained by calculating the circuit analogue described in section 2.

For the currents attracted at the two spherical electrodes (either electron or ion currents according to their polarity), we have used

$$i_j = i_{j0} f(\phi^*) \tag{13}$$

where $j = i, e$ for ions and electrons, respectively, $\phi^* = |eV/kTe|(\lambda_{de}/r)^{4/3}$, in which λ_{de} is the Debye length and V is the electrode potential, and where

$$i_{eo} = \frac{1}{8} n|e|v_{\text{the}} A \tag{14}$$

$$i_{io} = \frac{1}{4} nZ|e|V_0 A \tag{15}$$

are the electron and ion currents, respectively, which are geometrically collected, A being the collecting area. For the electrons we have a thermal collection, as the electron thermal velocity v_{the} is much larger than the tether (Shuttle) velocity ($v_0 = 7.8$ km/s). For the ions, on the other hand, the opposite is true, and consequently, i_{i0} is essentially a ram current.

The function $f(\phi^*)$, which is given in Figure 3, was calculated elsewhere [*Anderson et al.*, 1979]

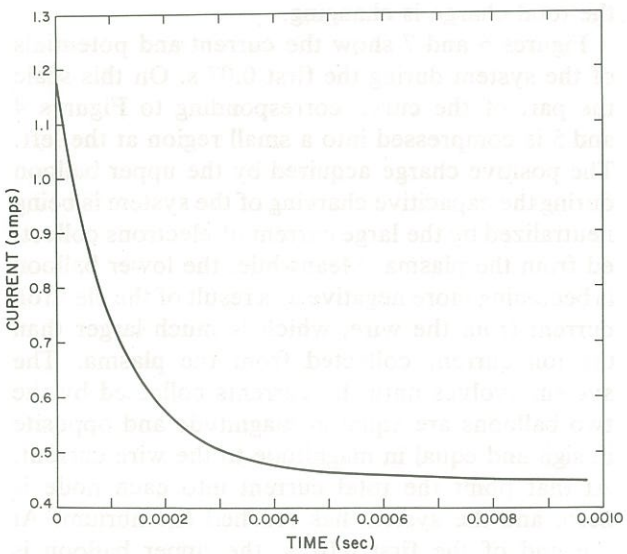

Fig. 4. Wire current versus time during the capacitive charging phase.

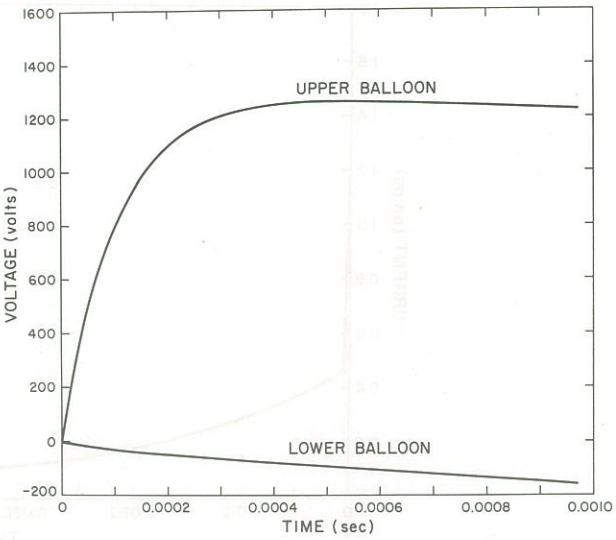

Fig. 5. Electrostatic potential of the balloon versus time during the capacitive charging phase.

by extrapolating results of *Alpert et al.* [1965] and *Linson* [1969] for particle collection from electrodes at high potentials ($eV/kT \gg 1$). As is seen from Figure 3, at such large potentials the current can be much higher than the geometrical currents (14) or (15).

As far as capacitance of the end electrodes is concerned, in the calculations presented here we have been using $C = 4\pi\varepsilon_0 r_1 r_2/(r_2 - r_1)$, the capacitance of a spherical condenser, by choosing $r_2 - r_1$ of the order of the Debye length. This is not correct in the case of an electrode at high potential, where the dimensions of the charged sheaths surrounding the electrode could be many Debye lengths [*Alpert et al.*, 1965; *Mlodnosky and Garriot*, 1963]. However, the purpose of the results presented here is that of illustrating the capacity of the circuit analogue method to perform transient calculations and that of illustrating the general features of such transients rather than describing a given case in an accurate quantitative way.

Some typical results are illustrated in Figures 4–7. These results were obtained using a computer model that integrates the dynamics of long wires in space [*Anderson et al.*, 1979]. The physical system consists of a 10-km, coated wire with a 10-m radius balloon at the lower end and a 1.668-m radius balloon at the upper end. The upper balloon, whose size is chosen to approximate the area of the metal

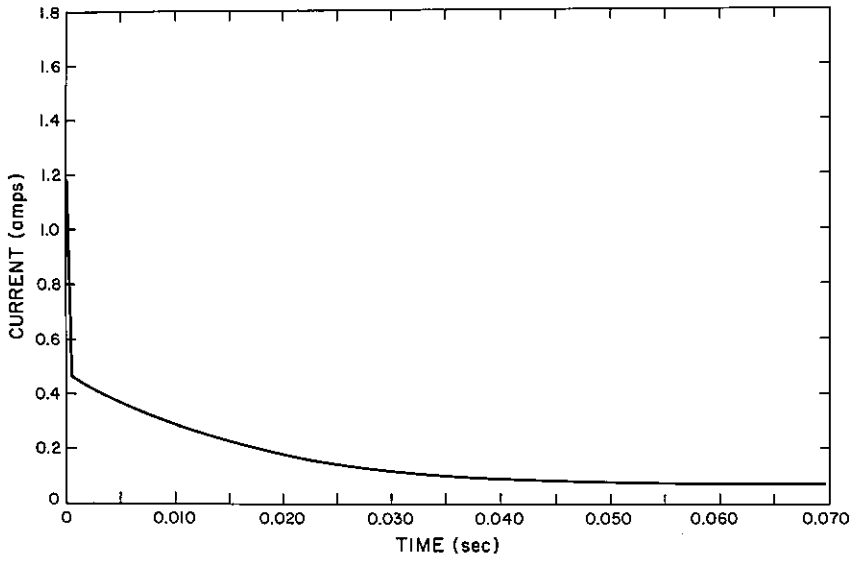

Fig. 6. Wire current versus time as the system establishes equilibrium with the ionosphere.

surfaces of the space shuttle, is at an altitude of 220 km in an equatorial orbit. The resistance of the wire is 1909.859 Ω (piano steel wire). The capacitance used for the upper balloon is 0.85×10^{-7} F, and the capacitance of the lower balloon is 0.303×10^{-5} F. The circuit analogue used in the calculations consists of only two nodes representing the balloons with a resistor between them. The capacitance of the wire has been neglected.

Figure 4 shows the wire current versus time during the first millisecond. Figure 5 shows the voltage of the upper balloon and the lower balloon for the same time period. The initial charge on the capacitors is zero. Since there is no initial electrostatic potential difference, the current starts out at the resistively limited value of 1.174 A, obtained by dividing the induced voltage of 2242.3 V by the wire resistance. As current flows the balloons become charged up, as shown in Figure 5. Since the capacitance of the upper balloon is much smaller than that of the lower balloon, it acquires a large positive potential, and the lower balloon acquires a small negative potential. As the balloons become charged, the electrostatic potential opposes the induced voltage, and the current drops. At the end of the first millisecond the upper balloon is at 1224.9 V and is collecting an electron current of −0.45470 A. The lower balloon is at −164.4 V and is collecting an ion current of 0.02624 A. The wire current is 0.44662 A, giving a resistive potential drop of 853 V. This first phase is the capacitive charging of the system. If there were no leakage to the plasma, the system would be essentially in equilibrium at the end of the first millisecond. However, using the formulas for collection efficiencies [see (13)–(15) and Figure 3], we see that the upper balloon is collecting a much larger electron current than the ion current collected by the lower balloon, so that the total charge is changing.

Figures 6 and 7 show the current and potentials of the system during the first 0.07 s. On this scale the part of the curve corresponding to Figures 4 and 5 is compressed into a small region at the left. The positive charge acquired by the upper balloon during the capacitive charging of the system is being neutralized by the large current of electrons collected from the plasma. Meanwhile, the lower balloon is becoming more negative as a result of the electron current from the wire, which is much larger than the ion current collected from the plasma. The system evolves until the currents collected by the two balloons are equal in magnitude and opposite in sign and equal in magnitude to the wire current. At that point the total current into each node is zero, and the system has reached equilibrium. At the end of the first 0.07 s, the upper balloon is at +5.4614 V and is collecting an electron current of −0.069402 A. The lower balloon is at

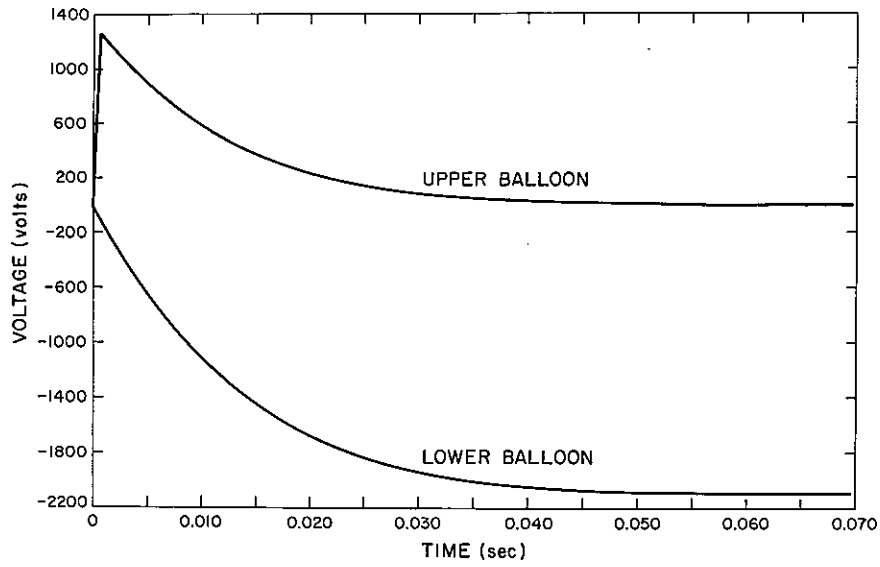

Fig. 7. Electrostatic potential of the balloon versus time as the system establishes equilibrium with the ionosphere.

$-0.2104.3713$ V and collecting an ion current 0.068731 A. The wire current is 0.069396 A, and the system is nearly in equilibrium at this point.

4. EQUILIBRIUM CURRENT AND POTENTIAL PROFILES IN BARE METALLIC TETHERS

The results presented in this section refer to a tether of length $L = 100$ km and radius $r_w = 0.5$ mm. We also use $v_0 = 7$ km/s and $B_0 = 0.5$ G, giving a total potential drop $\Delta\phi_0$ for a perfectly conducting wire of 35 kV. (Actually, for a Shuttle-borne tether, more appropriate values would be $B \simeq 0.3$ G and $\Delta\phi_0 \simeq 20$ kV. We have employed the above values here in order to compare our results with those of *Dobrowolny* [1978].) Finally, we refer to the case of a tether deployed downward from the shuttle at a nominal altitude of 220 km and use $n \simeq 6.28 \times 10^{11}$ m^{-3} for the electron density and $T \simeq 0.18$ eV for the electron temperature.

The current per unit length attracted from the plasma by a point of the wire at potential V is calculated from

$$i_j^a = 2r_w neZ_j \sqrt{\frac{\pi}{4} v_{thj}^2 + v_0^2} \cdot \left[2\sqrt{\frac{\eta_j}{\pi}} + (1 - \operatorname{erf}\sqrt{\eta_j}) e^{\eta_j} \right] \tag{16}$$

where e is the electron charge, v_{thj} is the thermal velocity of species j particles ($j = i$ for ions and $j = e$ for electrons), $Z_i = 1$ for singly ionized oxygen atoms in the ionosphere, and η_i is a dimensionless potential given by

$$\eta_j = \frac{|eV/kT_j|}{1 + (4/\pi)(v_0/v_{thj})^2} \tag{17}$$

The attracted current will be an ion current for those portions of the wire where $V < 0$ and an electron current where $V > 0$. The current repelled by the wire is given by

$$i_j^r = |2r_w neZ_j| \sqrt{\frac{\pi}{4} v_{thj}^2 + v_0^2}\, e^{-\eta_j} \tag{18}$$

The function $f(V_i)$ introduced in (2), i.e., the total current from the plasma, will then be the ion current minus the electron current.

Equation (16) for the attracted current corresponds to the orbital-motion-limit approximation of *Langmuir and Mott-Smith* [1961]. It is equivalent to the formulation used in *Dobrowolny* [1978] and others [*Hoegy and Wharton*, 1972; *Shkarofsky*, 1972]. A discussion of the validity of this approx-

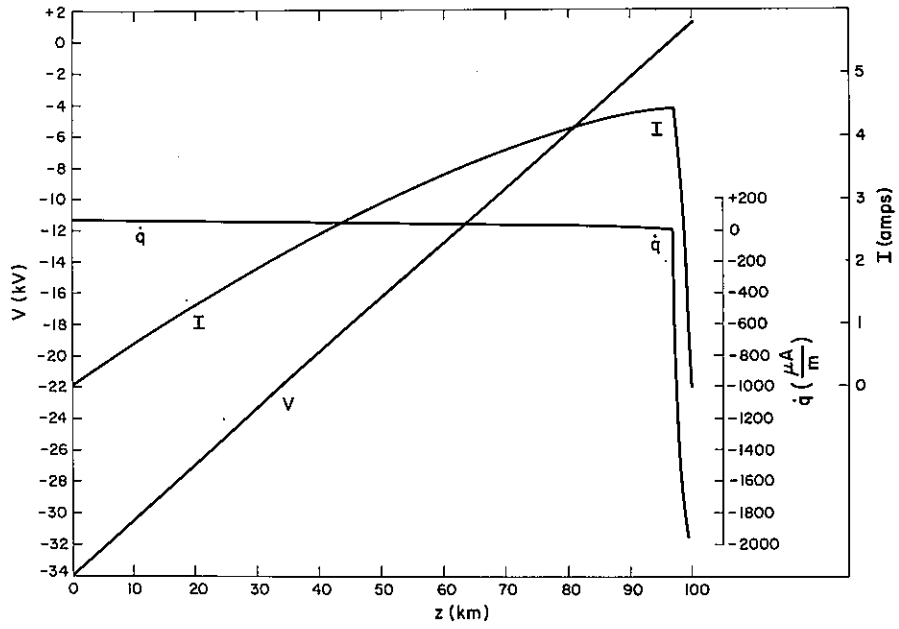

Fig. 8. Voltage, current, and charge distribution for a 100-km bare wire with zero resistance.

imation for the case under consideration here is contained in *Dobrowolny et al.* [1976].

In the limit of very high potential, $eV/kT \gg 1$, which would be expected along most of the tether, the attracted current simplifies to

$$i_j^a \simeq 2r_w n|e|v_{\text{th}j}\sqrt{\eta_j} \tag{19}$$

which corresponds to the model used by *Morrison et al.* [1979] and, indeed, is a very good approximation everywhere along the wire except in the immediate vicinity of zero potential.

In Figure 8, we show the profiles of voltage, current, and charge distribution corresponding to a perfectly conducting tether. The maximum current is ~4.4 A. The zero potential is found about 3 km from the top of the 100-km wire; most of the wire therefore is negative with respect to the plasma, with only the top 3 km being positive. This is in agreement with what is found by using Dobrowolny's equations for the same parameters.

Figure 9 gives the profiles with the resistance of the wire taken into account; this case refers to an alloy steel wire of resistivity $\rho = 0.15$ μΩ m, and thus the total resistance of the wire is $R = 19.1$ kΩ. As seen, values of the maximum current (~1.75 A) and potential are reduced, but the general behavior of the profiles remains the same as in the case of zero resistance.

We repeated our dynamic calculation using the parameters from *Dobrowolny*'s [1978] Figures 5 and 6. The voltage profile is similar to his Figure 6, but the current profile is quite different. Rather than current spikes or reversals, we get a current that is constant at ~1.8326 A for a section about 70 km long in the middle of the wire and goes to zero at both ends (the 1.8326-A current corresponds to the current v_0BL/R determined by resistance). We discuss these discrepancies in the next section.

Assuming now a resistivity of $\rho = 1.5$ μΩ m, i.e., a total resistance of 191 kΩ (stainless steel wire), we obtain the profile shown in Figure 10. For such high resistance, the current is resistivity-limited to the maximum value $i_{\max} = 0.18326$ A over most of the wire, which is what is obtained from

$$i_R = \frac{v_0 BL}{R} \tag{20}$$

In other words, there is no current leakage from the plasma along most of the wire. Correspondingly,

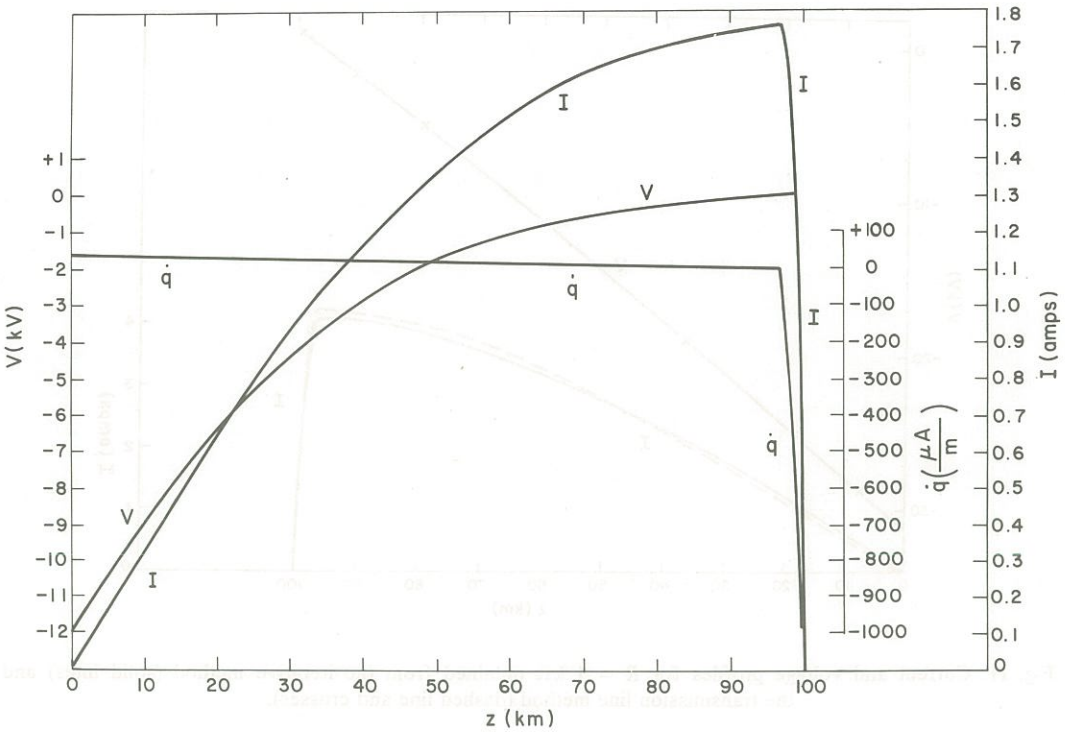

Fig. 9. Voltage, current, and charge distribution for a 100-km bare wire with 19.1-kΩ resistance ($\rho = 0.15$ $\mu\Omega$ m).

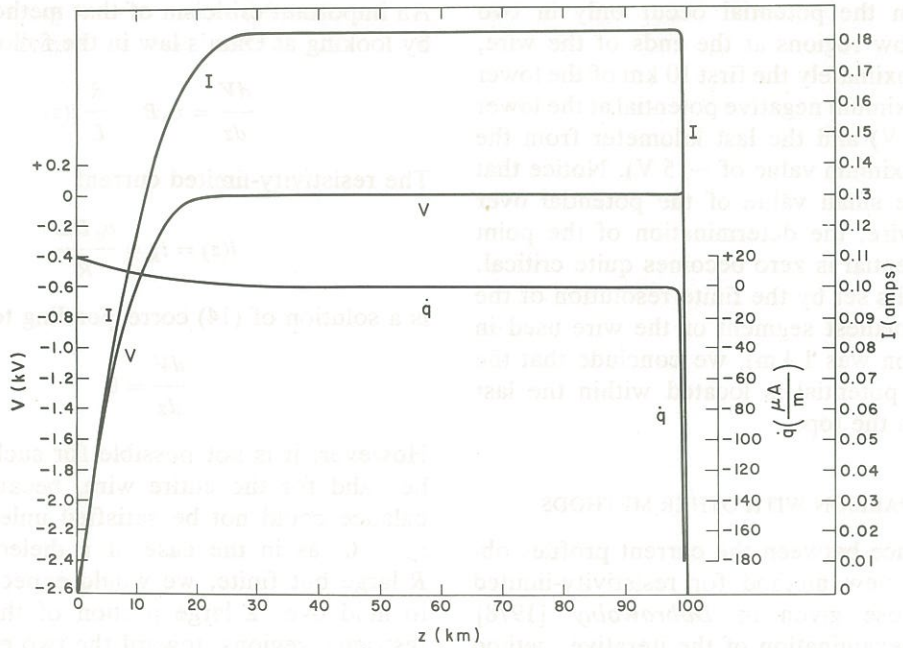

Fig. 10. Voltage, current, and charge distribution for a 100-km bare wire with 191-kΩ resistance ($\rho = 1.5$ $\mu\Omega$ m).

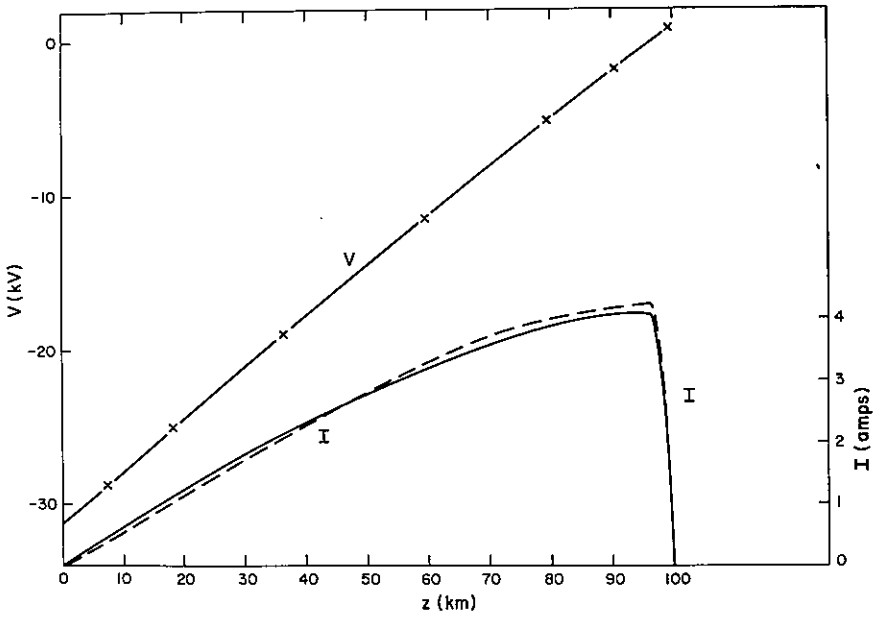

Fig. 11. Current and voltage profiles for $R = 1$ kΩ obtained from the iterative method (solid lines) and the transmission line method (dashed line and crosses).

the potential in such a resistivity-limited section is very small (−0.6233 V) and $\dot{q} = 0$.

Variations in the potential occur only in two relatively narrow regions at the ends of the wire, i.e., over approximately the first 10 km of the lower end (with a maximum negative potential at the lower end of −2600 V) and the last kilometer from the top (with a maximum value of ~15 V). Notice that because of the small value of the potential over most of the wire, the determination of the point where the potential is zero becomes quite critical. Within the limits set by the finite resolution of the method (the smallest segment of the wire used in the computation was 1 km), we conclude that the point of zero potential is located within the last kilometer from the top.

5. COMPARISON WITH OTHER METHODS

The difference between the current profiles obtained by the new method for resistivity-limited cases and those given in *Dobrowolny* [1978] prompted a reexamination of the iterative method used by Dobrowolny. In his approach, he started with current and potential profiles corresponding to $R = 0$ and arrived at the real value of the wire's resistance by gradually increasing the resistance. An important criticism of that method can be seen by looking at Ohm's law in the following form:

$$\frac{dV}{dz} = v_0 B - \frac{R}{L} i(z) \tag{21}$$

The resistivity-limited current

$$i(z) = i_R = \frac{v_0 BL}{R} \tag{22}$$

is a solution of (14) corresponding to

$$\frac{dV}{dz} = 0 \tag{23}$$

However, it is not possible for such a solution to be valid for the entire wire, because the charge balance could not be satisfied unless $R = \infty$ and $i_R = 0$, as in the case of a dielectric wire. For R large but finite, we would expect (22) and (23) to hold over a large portion of the wire, but in restricted regions, toward the two ends, we would find variations in the potential, as indicated by the V profile in Figure 5.

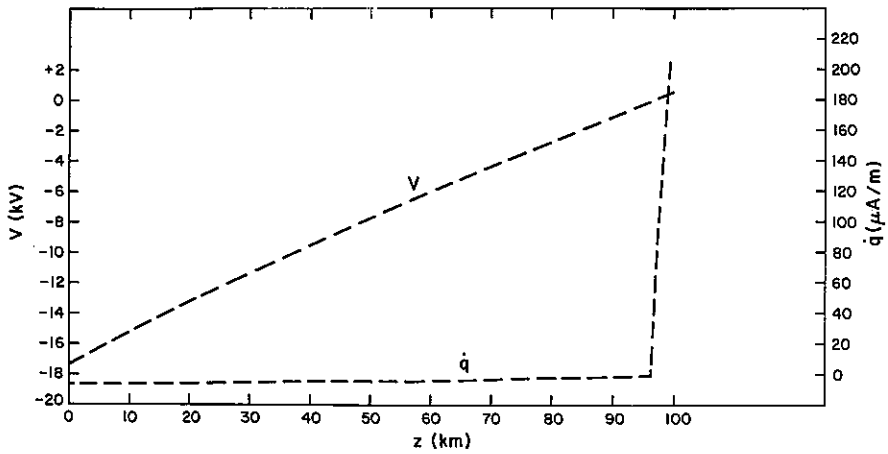

Fig. 12. Voltage and charge variation for parameters corresponding to Figure 7b from *Morrison et al.* [1979].

Now, in the jth step of the iterative method, (21) can be replaced by

$$\frac{dV_j}{dz} = \frac{dV_{j-1}}{dz} - \frac{\Delta R_j}{L} i_{j-1}(z) \tag{24}$$

where $V_j(z)$ is the potential profile obtained in terms of the profiles of potential $V_{j-1}(z)$ and current $i_{j-1}(z)$ from the previous iterative step, and ΔR_j is the increment in resistance at the jth step. At each stage of the iteration we must make sure that

$$\frac{dV_j}{dz} \geq 0 \tag{25}$$

i.e., that the potential maintains monotonic behavior.

Clearly, if we want to approach a resistivity-limited case, where (23) would be approximately true over a large portion of the wire, condition (25) requires that (24) be calculated in infinitesimally small iterative steps. The iterative method, then, becomes completely impractical in cases where the current is resistivity limited, such as that treated in *Dobrowolny* [1978]. We now believe that the spikes and reversals obtained iteratively in Dobrowolny's current profile were mainly due to the fact that from a certain point, the iteration steps were not small enough to satisfy (25) and hence caused incorrect results.

In Figure 11, we show current and potential profiles obtained with the iterative method (solid lines) for $R = 1$ kΩ (a case not resistively limited) and the same profiles obtained with the transmission line model presented in this paper (dashed lines and crosses). We see that there is good agreement between the two results. In particular, agreement for the potential is so good that the curves are indistinguishable; the crosses are the numbers obtained with the transmission line model. However, the present dynamic formulation which is able to test correctly the resistive cases and in addition calculate transient behavior clearly supercedes the previous work of Dobrowolny.

It should also be pointed out that the differential problem solved by *Morrison et al.* [1979] does not appear directly applicable to cases of very high resistance. The reason is that their model for the flux of attracted particles (see (12)) is correct only for large potentials and hence fails for those portions of the wire that are resistivity limited and where the potential is very small ($V = -0.622$ V in Figure 10). Even in these cases, however, their model can be employed (see appendix) to determine the approximate thickness of the small regions at the extreme ends of the wire, where the potential variations are localized. Note that the cases treated by *Morrison et al.* [1979] are not resistivity limited in the sense of Figure 10. We show in Figure 12 results obtained with the transmission line model, for which we used the same parameters as in Figure 7b of *Morrison et al.* [1979]; our results agree well with theirs.

In conclusion, with respect to methods previously used, the transmission line model presented here appears to be the only one capable of calculating current and potential profiles for cases of high

resistance of the tether, such that the current has the resistivity-limited value given by (22) over a large portion of the tether. At the same time, our model agrees well with the other two methods when the tether resistance has only moderate effects.

APPENDIX: AN APPROXIMATE BOUNDARY LAYER SOLUTION FOR HIGH-RESISTANCE TETHERS

Differentiating (21) and using (19) for the current of attracted particles, if the repelled particle contribution to the current is neglected, we get the differential equation for V used by *Morrison et al.* [1979]. In dimensionless terms this can be written

$$\varepsilon_j \frac{d^2\tilde{\phi}_j}{d\zeta^2} = -(\tilde{\phi}_j)^{1/2} \tag{A1}$$

where $\zeta = z/L$, $\tilde{\phi}_j = |eV/kT_j|$, and

$$\varepsilon_j = \frac{1}{R}\frac{kT_j}{en}\frac{1}{2r_w L v_{thj}} \tag{A2}$$

Here, $j = i$ in the region of negative potential, and $j = e$ in the region of positive potential.

As indicated in the main body of the paper, (A1) cannot be used for cases of high resistance for that portion of the tether where the potential is very small and the current is resistivity limited. It can, however, still be used as an approximation for the restricted regions where there are potential variations (see Figure 10). For high resistance we have $\varepsilon_j \ll 1$, and (A1) clearly gives rise to a boundary layer problem [*Cole*, 1968]. For example, for $R = 191$ kΩ (the value for the profiles of Figure 10) we have $\varepsilon_i = 4.3 \times 10^{-5}$ and $\varepsilon_e = 1.1 \times 10^{-6}$.

Introducing the following variable

$$\zeta_j = \zeta/\varepsilon_j \tag{A3}$$

to obtain variations over very short intervals, (A1) becomes

$$\frac{1}{\varepsilon_j}\frac{d^2\phi_j}{d\zeta_j^2} = -(\tilde{\phi}_j)^{1/2} \tag{A4}$$

so that on the scale ζ_j we get, to the lowest order,

$$\frac{d^2\tilde{\phi}_j}{d\zeta_j^2} = 0 \tag{A5}$$

and hence near the ends of the wire there will be two regions of approximately linear variation of the potential. Furthermore, we know the slope of the linear variation, because as the current goes to zero at the extremes of the wire, (21) gives

$$\left(\frac{dV}{d\zeta}\right)_{\zeta=0} = \left(\frac{dV}{d\zeta}\right)_{\zeta=1} = v_0 BL \tag{A6}$$

This information is now sufficient to estimate the approximate thickness of the two regions where the potential variations are localized and the current is below the resistive value (20). We can obtain the widths $\Delta\zeta_i$ and $\Delta\zeta_e$ of the negative and positive regions, respectively, from the condition that the currents collected in each of them must equal the resistive current (20). In this way, we get

$$r_w Ln|e| v_{thj} \tilde{\phi}_0^{1/2} (\Delta\zeta_j)^{3/2} = i_R \tag{A7}$$

where $\tilde{\phi}_0 = v_0 BL/kT$. We then see that $\Delta\zeta_j$ scales as $R^{-2/3}$; furthermore, for $T \sim 0.18$ ev, $\Delta z_i/\Delta z_e \sim 40$ (i.e., the negative region is always wider than the positive one). Using the parameters from the calculations in Figure 5, we find

$$\Delta z_i \sim 8 \text{ km} \qquad \Delta z_e \sim 200 \text{ m} \tag{A8}$$

Taking into account the approximate nature of the solution, which is really valid in a layer much smaller than Δz_j, these results compare rather well with those obtained with the transmission line model and shown in Figure 10.

Finally, using the two widths and the slope $v_0 B$ of the approximate potential variation in these two regions, we can estimate the values of the potential at the two extremes of the wire as

$$V(z = 0) = -2.8 \text{ kV} \qquad V(z = 100 \text{ km}) = 70 \text{ V} \tag{A9}$$

The value at $z = 0$ is in very good agreement with that in Figure 10. Figure 10 gives a lower value of the potential at $z = 100$ km, because the region of nonzero potential is about a factor of 5 smaller than the 1-km resolution used in the transmission line model.

Acknowledgments. We thank M. D. Grossi for many discussions on the subject of this paper. This work was supported in part by contracts NAS8-31678 and NAS5-25077 from the National Aeronautics and Space Administration.

REFERENCES

Alpert, Ya-L., A. V. Gurevich, and L. P. Pitaevskii (1965), Space physics with artificial satellites, Consultants Bureau, New York.

Anderson, M. P., D. A. Arnold, G. Colombo, M. Dobrowolny,

M. D. Grossi, and L. R. Kirschner (1979), Orbiting tether's electrodynamic interactions, final rep. contract NAS5-25077, Smithsonian Astrophys. Observ., Cambridge, Mass.

Cole, J. D. (1968), *Perturbation Methods in Applied Mathematics,* Blaisdell, Waltham, Mass.

Dobrowolny, M. (1978), Electrodynamics of long metallic tethers in the ionospheric plasma, *Radio Sci., 13,* 417–424.

Dobrowolny, M., G. Colombo, and M. D. Grossi (1976), Electrodynamics of long tethers in the near-earth environment, *Rep. Geoastron. 3,* Smithsonian Astrophys. Observ., Cambridge, Mass.

Dobrowolny, M., D. A. Arnold, G. Colombo, and M. D. Grossi (1979), Mechanisms of electrodynamic interactions between a tethered satellite system and the ionosphere, *Rep. Radio Geoastron. 6,* Smithsonian Astrophys. Observ., Cambridge, Mass.

Drell, S. D., H. M. Foley, and M. A. Ruderman (1965), Drag and propulsion of large satellites in the ionosphere: An alfvenic propulsion engine in space, *J. Geophys. Res., 70,* 3131–3165.

Hoegy, W. R., and L. E. Wharton (1972), Current to a moving cylindrical electrostatic probe, *NASA Tech. Memo. TM X-66177.*

Langmuir, I., and H. M. Mott-Smith (1961), The theory of collectors in gaseous discharges, in *The Collected Works of Irving Langmuir,* vol. 4, edited by C. G. Suits and H. E. Way, pp. 99–132, Pergamon, New York.

Linson, L. M. (1969), Current-voltage characteristics of an electron-satellite in the ionosphere, *J. Geophys. Res., 74,* 2368–2375.

Mlodnosky, R. F., and O. K. Garriott (1963), The VLF admittance of a dipole in the ionosphere, in *Proceedings of the International Conference on the Ionosphere,* Institute of Physics and the Physical Society, London, 1963.

Morrison, P. J., W. B. Thompson, and P. R. Williamson (1979), Current collection by a long wire in near-earth orbit, submitted to *IEEE Trans. Plasma Sci.*

Shkarofsky, I. P. (1972), Nonlinear sheath admittance, currents, and charges associated with high peak voltage drive on a VLF/ELF dipole antenna moving in the ionosphere, *Radio Sci., 7,* 503–523.